International Journal of Hyperthermia

ISSN: 0265-6736 (Print) 1464-5157 (Online) Journal homepage: http://www.tandfonline.com/loi/ihyt20

Effect of practical layered dielectric loads on SAR patterns from dual concentric conductor microstrip antennas

F. Rossetto, P. R. Stauffer, V. Manfrini, C. J. Diederich & G. Biffi Gentili

To cite this article: F. Rossetto, P. R. Stauffer, V. Manfrini, C. J. Diederich & G. Biffi Gentili (1998) Effect of practical layered dielectric loads on SAR patterns from dual concentric conductor microstrip antennas, International Journal of Hyperthermia, 14:6, 553-571, DOI: 10.3109/02656739809018254

To link to this article: http://dx.doi.org/10.3109/02656739809018254

INT. J. HYPERTHERMIA, 1998, VOL. 14, NO. 6, 553–571

Effect of practical layered dielectric loads on SAR patterns from dual concentric conductor microstrip antennas

F. ROSSETTO†, P. R. STAUFFER†*, V. MANFRINI§, C. J. DIEDERICH† and G. BIFFI GENTILI‡

† Radiation Oncology Department, University of California, San Francisco, CA 94143-0226, USA
‡ Department of Electrical Engineering, University of Florence, Italy
§ Hewlett Packard Corporation, Bergamo, IT, USA

(*Received 5 February 1998; revised 9 June 1998; accepted 10 June 1998*)

Radiation patterns of 2 and 4 cm square Dual Concentric Conductor (DCC) microstrip antennas were studied theoretically with Finite Difference Time Domain (FDTD) analysis and compared with experimental measurements of power deposition (SAR) in layered lossy dielectric loads. Single and array configurations were investigated with 915 MHz excitation applied across either one, two or four sides, or four corners of the square apertures. FDTD simulations were carried out for realistic models of a muscle tissue load coupled to the DCC antennas with a 5 mm thick bolus of either distilled water or low loss Silicone Oil. This study characterizes the effect on SAR of adding three additional thin dielectric layers which are necessary for clinical use of the applicator. These layers consist of a 0.1 mm thick dielectric coating on the array surface to provide electrical isolation of DCC apertures, and 0.15 mm thick plastic layers above and below the bolus to contain the liquid. Experimental measurements of SAR in a plane 1 cm deep in muscle phantom agree well with theoretical FDTD simulations in the multi-layered tissue models. These studies reveal significant changes in SAR for applicator configurations involving low dielectric constant (ε_r) layers on either side of a high ε_r water bolus layer. Prominent changes include a broadening and centring of the SAR under each aperture as well as increased SAR penetration in muscle. No significant differences are noted between the simple and complete load configurations for the low ε_r Silicone Oil bolus. Both theoretical and measured data demonstrate relatively uniform SAR distributions with > 50% of maximum SAR extending to the perimeter of single and multi-aperture array configurations of DCC applicators when using a thin 5 mm water or Silicone Oil bolus.

Key words: Microwave array applicators, FDTD analysis, microstrip antennas, hyperthermia, SAR.

1. Introduction

Hyperthermia, which consists of heating tumours at a temperature of 42–45°C for about 1 h, has been shown capable of enhancing the effects of common anticancer treatments such as radiotherapy and chemotherapy (Sneed and Phillips 1991, Kapp 1996, Overgaard *et al.* 1996, Vernon *et al.* 1996). The Dual Concentric Conductor (DCC) microwave antenna analysed in this effort is intended to be used in large multi-aperture arrays for treatment of diffuse superficial tumours typically found in patients with chestwall recurrence of breast carcinoma. Effective heat treatment for this kind of disease requires an applicator capable of treating

* To whom correspondence should be addressed.

0265-6736/98 $12.00

irregularly shaped and often widespread disease extending from the skin surface to a maximum depth of about 1 cm. While previously used microwave applicators operating at either 915 or 433 MHz have demonstrated appropriate SAR penetration for generating effective heating to a depth of 1–1.5 cm (Chou *et al.* 1990, Straube *et al.* 1990, Gopal *et al.* 1992, Diederich and Stauffer 1993, Lee 1995), treatment of the entire disease is frequently impossible due to limited applicator size and poor coupling of rigid planar structures to the skin surface. Because superficial chestwall disease often wraps around complex body contours, the applicator must also be lightweight and flexible for complete uniform coverage of large areas while remaining comfortable for the patient during long treatments. A conformal microwave applicator made from an array of DCC apertures etched on the front surface of thin and flexible printed circuit board (PCB) material and excited at 915 MHz by microstrip feedlines etched on the PCB back surface has all the above characteristics and thus constitutes the subject of this investigation.

The Finite Difference Time Domain (FDTD) numerical method is an accurate tool for problems involving calculation of electromagnetic radiation in layered dielectric loads, and thus is useful for the design optimization of DCC applicators. Previous FDTD modelling efforts of this group have focused on studying various aperture sizes and electromagnetic feed configurations of single and multi-aperture arrays of DCC radiators placed in direct contact either with a lossy tissue load or with a coupling bolus which is itself in direct contact with the tissue. The direct coupling of liquid bolus to antenna and load, without any consideration for unavoidable dielectric interface layers to insulate the PCB copper surface and contain the liquid bolus, gave a reasonable model for initial theoretical investigations. While these field simulations agreed reasonably well with measured SAR distributions for some test conditions (Stauffer *et al.* 1994, 1995, 1996, 1998, Manfrini *et al.* 1995), the SAR measurements showed a tendency to spread further than the predicted fields. Thus it was felt important to look at a more complex FDTD load model which would take all the layers into account.

The present effort investigates the effect on radiated field patterns of three additional dielectric layers that must be used to insulate the applicator and contain the liquid bolus. Using this more complete model of the antenna load, the FDTD method is used to study two DCC aperture sizes (2 and 4 cm square) and two significantly different coupling bolus materials (distilled water and silicone oil) that appear suitable for clinical hyperthermia applications. For each of the above conditions, the theory is used to calculate SAR distributions for several physically realizable aperture excitation schemes. Following validation of the accuracy of single aperture simulations with measured SAR patterns from corresponding prototype antennas, results of six aperture array simulations are presented to demonstrate the appropriate interelement spacing required to obtain >50% SAR_{max} coverage out to the perimeter of multiaperture arrays.

2. Methods

2.1. *FDTD model of applicator and load*

The outline of a single square DCC aperture with excitation across one side gap is shown in figure 1a on top of the multiple layer load which characterizes the intended application of heating superficial tissue under a dielectric coupling bolus. As concerns the FDTD model, the DCC aperture consists of two coplanar concentric conducting edges separated by a thin radiating gap. Two different size square

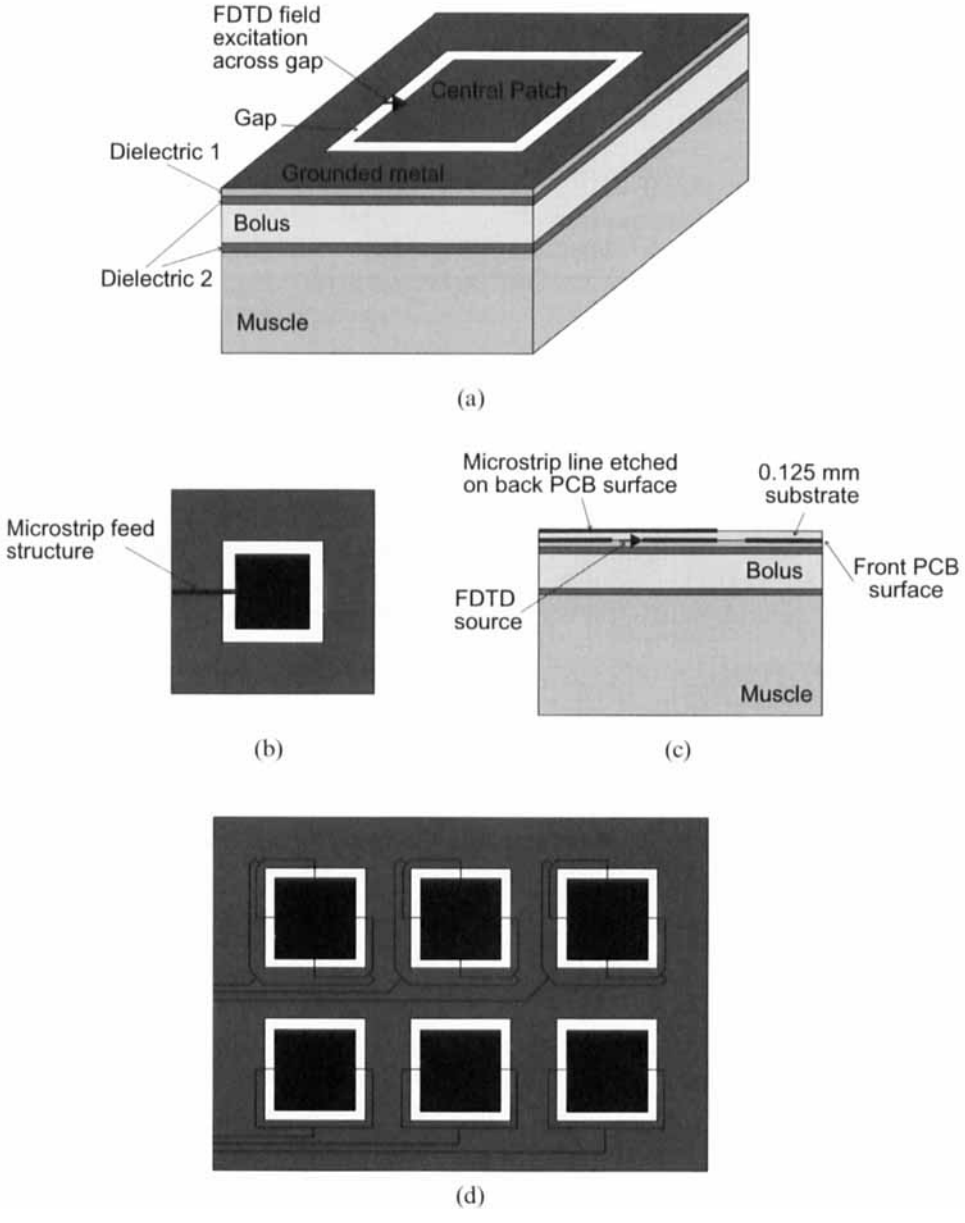

Figure 1. (a) Theoretical FDTD model of a single DCC aperture radiating into a layered dielectric load including: Dielectric 1 to insulate the copper aperture, Dielectric 2 on either side of the coupling bolus to contain the liquid bolus, and homogenous lossy muscle tissue load; (b) Model of a single aperture with feed structure consisting of a microstrip line crossing the gap and terminating with a square plate matching the size of the central patch of the DCC aperture; (c) Vertical section showing both the real microstrip and equivalent FDTD source placement for the case of one side feed aperture; (d) Model for array applicator with six apertures and examples of two different microstrip feedline configurations: the two side (bottom three apertures) and four side feed (top). The black metal represents the feedline network on the back surface of the PCB material, the grey metalization represents the PCB front surface, consisting of grounded metal rim and isolated patches located directly beneath the capacitively-coupled microstrip termination patches.

Table 1. Physical characteristics of the complete layered tissue load model.

Material	Thickness (mm)	Dielectric constant ε_r	Electrical conductivity σ (S/m)
Dielectric 1	0.1	3	0
Dielectric 2	0.15 (each layer)	7	0
Distilled water bolus	5	80	0.06
Silicone oil bolus	5	2.71	10^{-13}
Muscle tissue	30	56	1.4

apertures (2 and 4 cm slot length) were analysed in this study, with corresponding gap widths of 1 and 5 mm respectively. Radiation patterns were characterized for the single antenna and for six element array configurations shown in figure 1. For the single DCC structures, an infinite layer of metal around the square slot was simulated by extending the grounded metal layer for 7 cm beyond the aperture in both x and y directions to the end of the calculation domain. For the array calculations, a practical applicator was modelled by placing adjacent apertures 1.5 cm apart both horizontally and vertically, and including a finite 1.5 cm grounded metal rim around the array perimeter. Details of the corresponding prototype antenna construction are given in § 2.3.

For the FDTD simulations, the electromagnetic source excitation was modelled as a sinusoidal 915 MHz electric field applied directly across the gap either at the four corners, or at the centre of one, two, or four sides of the aperture. For array configurations, each of the elements was excited with noncoherent 915 MHz fields. This was realized by running six independent simulations of the entire 6-element array structure with only one element excited at a time, and then combining the six different power deposition patterns together according to the relation:

$$\mathrm{SAR}_{\mathrm{tot}}(x,y,z) = \sum_{i=1}^{6} SAR_i(x,y,z)$$

Appropriate consideration of available geometric aperture and source excitation symmetries allowed the study of just one quarter of the complete 18 cm long × 18 cm wide × 16 cm thick structure for the two and four side fed 4 cm square aperture. For the 2 cm aperture with single side feed, a single plane of symmetry allowed simulation of half the 16 × 16 × 16 cm structure. No symmetries were present for the six element arrays, which had model dimensions of 26 × 18.5 × 16 cm.

Figure 1a gives a schematic representation of the complete multi-layered load used for FDTD simulations. Model parameters are summarized in table 1. A tissue load extending well beyond the applicator edge was modelled by extending all layers horizontally an additional 3 cm beyond the aperture slot. Dielectric 1 represents a 0.1 mm layer of $\varepsilon_r = 3$ insulation which coats the PCB applicator surface to protect the copper. Dielectric 2 is the 0.15 mm thick polyurethane bag material ($\varepsilon_r = 7$) which contains the circulating temperature-regulated liquid coupling bolus. Two different dielectrics were considered for the 5 mm thick coupling bolus layer itself: distilled water ($\varepsilon_r = 80$) and low viscosity (50 cS) Silicone Oil ($\varepsilon_r = 2.71$). A 3 cm layer with $\varepsilon_r = 56$ and $\sigma = 1.4$S/m was used to simulate an infinitely thick muscle tissue load. A simpler load configuration without the use of additional interface

dielectrics was modelled using the 5 mm thick bolus in direct contact with DCC aperture and muscle load.

2.2. *FDTD numerical analysis*

The FDTD method consists of a discretization of the calculation domain into a large number of cells that are each a fraction of a wavelength and in which the electromagnetic fields are computed numerically by solving Maxwell's Equations in the time domain with a finite difference approximation of the partial derivatives in time and space (Yee 1966). Cell sizes of $\Delta x = \Delta y = 2.5$ mm were used everywhere except in the 1 mm gap region of the 2 cm aperture, where the cell size was reduced to 0.5 mm. This cell (2.5 mm) represents about $\lambda_{\text{eff}}/15$ in water where the smallest wavelength of 3.6 cm occurs, and about $\lambda_{\text{eff}}/18$ in muscle. In the vertical direction, cell height was varied from $\Delta z = 10$ mm in air above the applicator to $\Delta z = 2.5$ mm in muscle and bolus layers, and to ($\Delta z = 0.05$ mm in the thin dielectric layers. A non-uniform logarithmically changing grid size was used to connect the different discretization zones to avoid abrupt changes in adjacent cell size. For these conditions, the single 4 cm square aperture required 240 000 cells for the complete model and 80 000 cells without the interface dielectric layers. The six element arrays required 1 050 000 and 400 000 cells for 4 cm elements with and without layers respectively. To obey the Courant stability criterion (Umashankar and Taflove 1982), the number of time-steps per period at 915 MHz was 9200 and 450 for the 4 cm aperture with and without dielectrics respectively, and 9300 and 1700 for the 2 cm aperture. To avoid reflections and perturbation of the radiated field at the edges of the model, absorbing layers with progressively increasing conductivity were used at the domain boundaries, as suggested by Taflove (1980). Four layers with a thickness of four calculation cells each were used in the X and Y directions, for a total of 4 cm, and in the positive Z direction, for a total of about 12 cm. Due to the high losses typical of muscle tissue, no absorbing layers were used in the negative Z direction under the 3 cm thick muscle tissue load. A steady state analysis at 915 MHz was performed, enforcing sinusoidal electric fields across the aperture gap in the cells corresponding to positions directly under the PCB back surface microstrip feedlines. This simplified model of actual microstrip feedline excitation has been proven accurate in previous work (Stauffer *et al.* 1998). Steady state electric fields were calculated in all cells of the model and SAR was derived according to the relation:

$$SAR = \frac{\sigma \times E_{\text{tot}}^2}{2\rho} = \frac{\sigma}{2\rho}(E_x^2 + E_y^2 + E_z^2)$$

where ρ and σ represent the density and conductivity of the tissue load respectively.

2.3. *DCC applicator construction*

Prototype DCC applicators were constructed from a thin and flexible double-sided printed circuit board material in an array configuration with three rows and four columns of elements spaced 1.5 cm apart. The PCB material (Pyralux LF9131 from Dupont Electronic Materials Corp., Research Triangle Park, NC) used for each applicator was 0.125 mm thick, including polyimide substrate ($\varepsilon_r = 3.3$ and $\delta = 0.018$) and 0.036 mm thick copper on each side. The 4 cm DCC apertures were formed by etching a 5 mm wide slot around a 3 cm square central patch in the front surface copper layer, and the 2 cm apertures were formed similarly with a 1 mm wide slot around a 1.8 cm square patch. In both arrays 0.5 mm wide microstrip feedlines

spaced 1.5 mm apart centre to centre were etched from the rear surface copper layer, running in parallel directly over the front surface copper ground plane between apertures. The microstrips extended from coaxial PCB connectors (PCX connectors from Phoenix Connector Inc., Wood Dale, IL) on one edge of the PCB to individual aperture feed networks which excited the central patches by crossing the aperture slot at either one side (figures 1b and c), two or four sides (figure 1d), or four corners. After crossing the gap the feedlines were all connected to a central plate that matched the shape of the front surface square central patch. Once the two sides were etched and PCB connectors soldered to the feedlines and groundplane, the array was cleaned and both sides coated with an insulating dielectric ($\varepsilon_r = 3.0$) to electrically isolate, protect from corrosion, and simplify cleaning of the array.

The DCC antennas were coupled to the tissue equivalent phantom material with a 5 mm thick coupling bolus of either distilled water ($\varepsilon_r = 80$, $\sigma = 0.06$ S/m) or Silicone Oil (DC 200 Fluid 50cS from Dow Corning Corp, Midland, MI) ($\varepsilon_r = 2.7$, $\sigma = 10^{-13}$ S/m). For the tests in this paper, bolus containers suitable for the patient clinic were fabricated by heat seal forming appropriate size 'Bolus Bags' from a 0.15 mm thick durable but flexible polyurethane membrane ($\varepsilon_7 = 7$, $\sigma = 0$ S/m), with 5 mm thick low density filter foam used to maintain proper bolus shape and thickness. With two ports for circulating the temperature regulated liquid, all air was removed and excess fluid purged from the closed circuit to maintain a uniform 5 mm thick bolus layer.

2.4. *Experimental SAR measurements*

The SAR pattern of each aperture configuration was measured by scanning a three orthogonal axis electric field probe (Narda 8021B SAR Probe from Narda Microwave Corp. Hauppauge, NY) through a liquid muscle tissue equivalent phantom (Hartsgrove *et al.* 1987) contained in a $30 \times 38 \times 60$ cm Plexiglas tank. To characterize each aperture, approximately 5 watts of power was applied at 915 MHz and the miniature 4 mm diameter SAR probe scanned in 2.5 mm increments in a plane 1 cm in front of the bolus (1.5 cm from the DCC aperture surface). The accuracy and validity of this SAR mapping procedure have been described previously (Stuchly *et al.* 1984, Diederich and Stauffer 1993). The computer controlled scanner had a positional accuracy and precision of 0.5 and 0.2 mm respectively. The liquid muscle phantom was circulated vigorously throughout the scans which took approximately 20 min per aperture.

3. Results

The first configuration studied was the 4 cm aperture with 5 mm thick distilled water bolus and four side feed configuration. Figure 2 shows the SAR distribution in a horizontal plane 1 cm deep in muscle normalized to the maximum SAR value in that plane. In order to improve understanding of the complete radiated field, the SAR distribution is presented along with one of its component fields—the X-directed field normalized to the maximum total field squared (E_x^2/E_{TOT}^2). For symmetric four side and four corner feed configurations, E_y^2 is identical to the E_x^2 component except rotated by 90°. A lower central peak is also visible in figure 2a from the E_z^2 component which contributes at most 81% of the maximum E_{TOT}^2 field. The dashed squares represent the applicator gap superimposed to scale over the contour plots. If low ε_r dielectric layers are not considered between the applicator, bolus, and tissue layers (figures 2a and b), the SAR distribution is characterized by four peaks at the

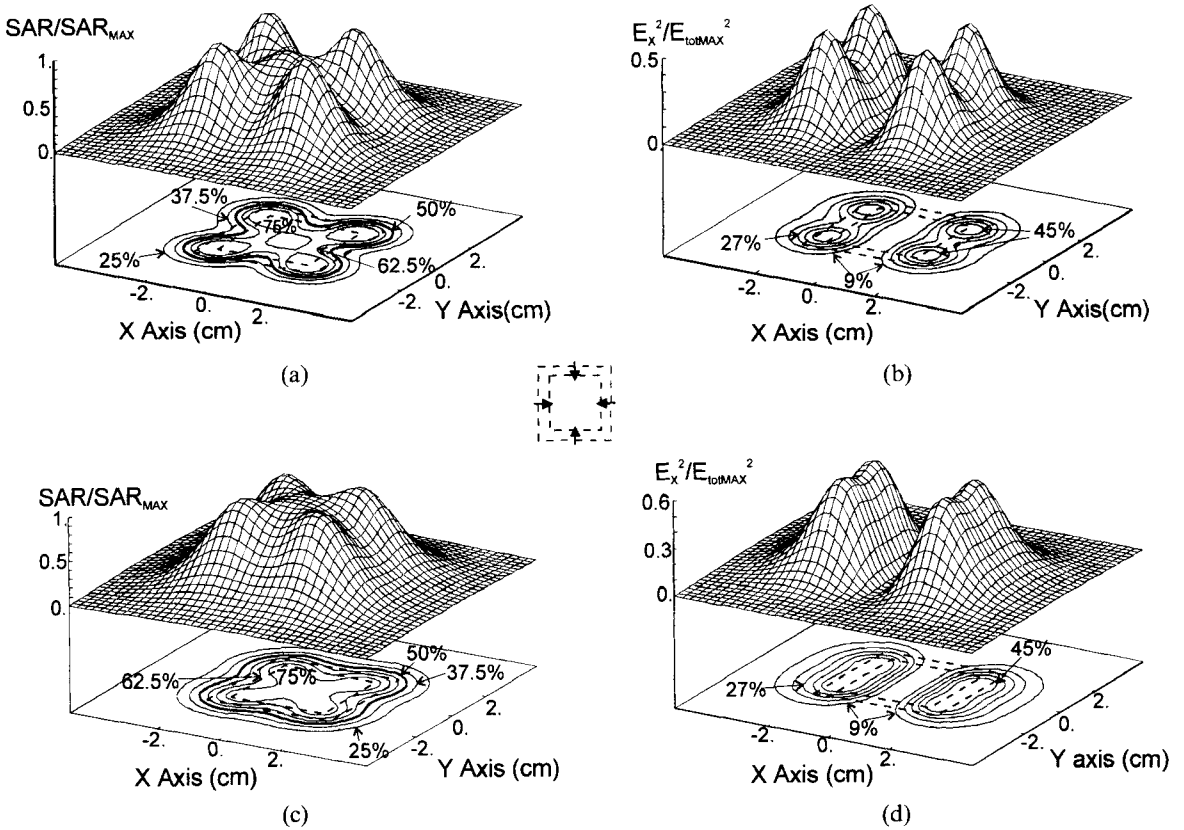

Figure 2. SAR and E_x^2 distributions for a 4 cm aperture with a four side feed and 5 mm thick water bolus in a horizontal x-y plane 1 cm deep in tissue. (a) and (b) SAR and E_x^2 when the water bolus is in direct contact with the applicator and tissue; (c) and (d) SAR and E_x^2 in the more realistic configuration with interface dielectrics between applicator, water bolus, and tissue. The dashed squares represent the aperture gap drawn to scale over the contour plot. Note the improved uniformity and lateral extent of SAR when thin low ε_r layers are included in the model.

aperture corners from the predominant X and Y component fields. For this direct coupled four side feed configuration, small portions of the aperture cross section near the middle of each side gap are not covered by the 50% SAR contour (bold line). The addition of thin dielectric layers to more accuractely model the applicator insulation and bolus bag materials has the effect of spreading and smoothing the power deposition pattern as shown in figures 2c and d. In this case, power deposition becomes even more uniform under the aperture face, and the 50% SAR contour expands to an almost square shape that completely covers the aperture perimeter. Figure 3 shows power deposition displayed in a vertical cross section through the aperture centre. SAR is normalized to the peak value in muscle, which is located at the bolus interface directly under one of the corner peaks so is not visible on this cross section. Figure 3 also shows that due to spreading of the corner SAR peaks, effective penetration of SAR is higher in the configuration with interface dielectrics, since the 10% SAR level extends almost 1 cm deep centrally instead of 3 mm deep for the same aperture without dielectric layers.

Figure 4 shows a comparison between FDTD and measured SAR results in the 1 cm deep plane for a single 4 cm aperture with 5 mm water bolus and all interface dielectric layers of figure 1a, when the centre patch is excited across two sides, four sides, or four corners. Note that for all three electromagnetic feed configurations, the results of FDTD theory are qualitatively very similar to the experimentally measured SAR patterns and the four side feed configuration appears to give the best coverage of the aperture with $\geq$50% SAR. Figure 5 shows simulated SAR 1 cm deep in muscle for a six element non-coherent array of 4 cm apertures spaced 1.5 cm apart, each with four side excitation and coupled to the muscle load with 5 mm water bolus and realistic low ε_r dielectric layers. The dashed aperture outlines are projected with appropriate scale and position on the contour plot. The 50% SAR contour line is seen to cover the entire perimeter of the six element array. Even the 62.5% SAR contour is continuous except for small holes between apertures which in the practical application will be filled in terms of temperature by thermal conduction effects.

Similarly, the 4 cm aperture was theoretically studied with 5 mm thick Silicone Oil bolus and dielectrics. In this case, the two side $(+/-X)$ feed was sufficient to produce the SAR distribution 1 cm deep in muscle shown in figure 6a. The pattern presents prominent peripheral peaks as a result of the high X and Y field components under the gaps, and a central hole down to about 60% of maximum SAR due to the lower magnitude centrally peaked Z component. The 50% SAR contour is continuous and covers the entire aperture face. SAR patterns obtained from 4 cm square apertures coupled to tissue using low ε_r Silicone Oil bolus instead of water are compared directly in planes 1 cm deep in muscle (figure 6b) and in the central vertical cross section (figure 6c) for cases with and without extra interface dielectrics. Note the similarity of SAR obtained with and without additional dielectric layers. Figure 7 shows the SAR distribution for a six element array of 4 cm apertures coupled with 5 mm Silicone Oil bolus. The SAR is quite uniform throughout the centre portion of the array with slight enhancement at the corners just outside the array boundary due to the effect of 1.5 cm ground plane rim around the apertures. While small holes are present in the 62.5% contour level, the 50% SAR completely covers the applicator face and conforms closely to the outer perimeter of the array.

The smaller 2 cm square DCC aperture, which represents only about $\lambda/2$ in muscle, was studied with a simple one side feed configuration. Figure 8a shows FDTD computed SAR distributions 1 cm deep in muscle under a 5 mm thick

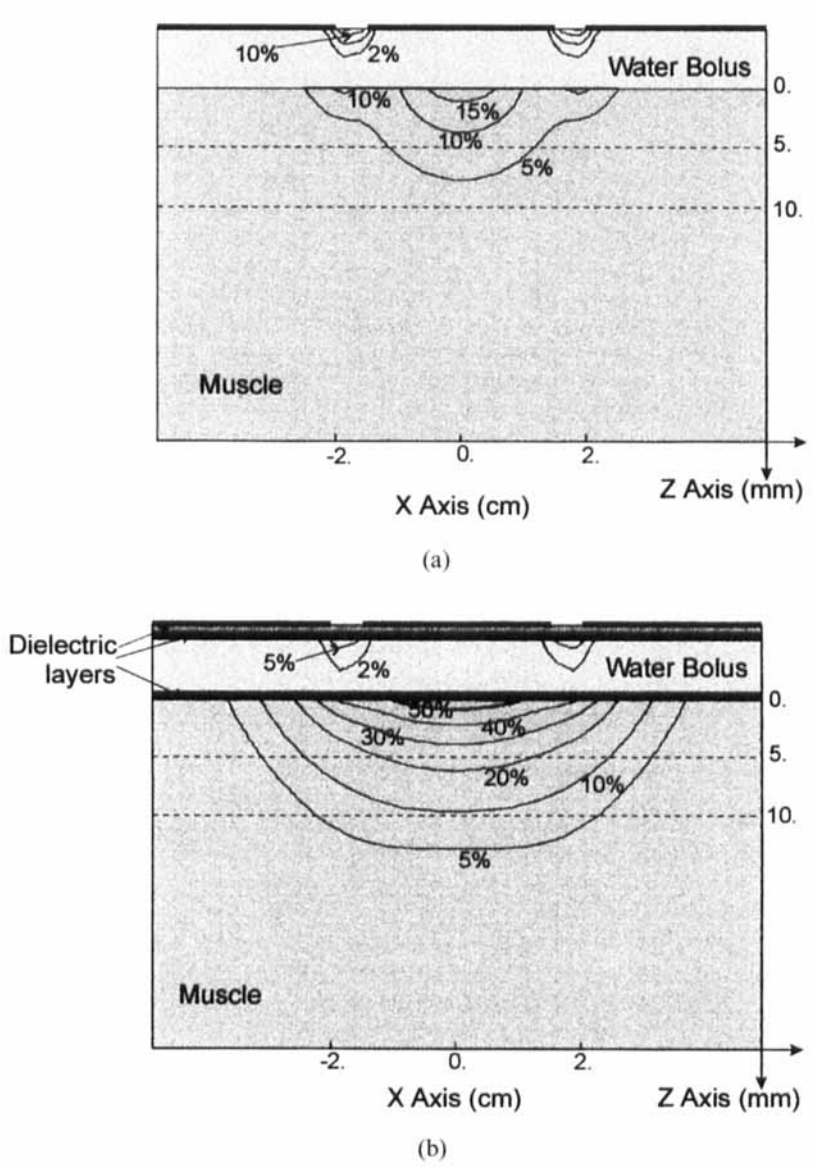

Figure 3. SAR contours in a vertical cross section through the centre of a 4 cm aperture excited across all four side gaps and coupled with 5 mm water bolus, without (a) and with (b) interface dielectrics. Note the significant increase of penetration depth when using the complete model. The plots are normalized to 100% SAR_{max} occurring in muscle under one corner of the aperture.

water bolus with (solid line) and without (dotted line) the three interface dielectrics. In both cases, there is a single central peak, slightly off-centre under the non-symmetrically fed apertures. With the intervening dielectrics, the 50% contour is considerably smoother, more symmetric, and covers almost the entire aperture perimeter except for a small portion of each corner. By comparison, the SAR pattern obtained without interface dielectrics results in significantly poorer symmetry, with the power deposition peak shifted away from aperture centre off to the side with the microstrip

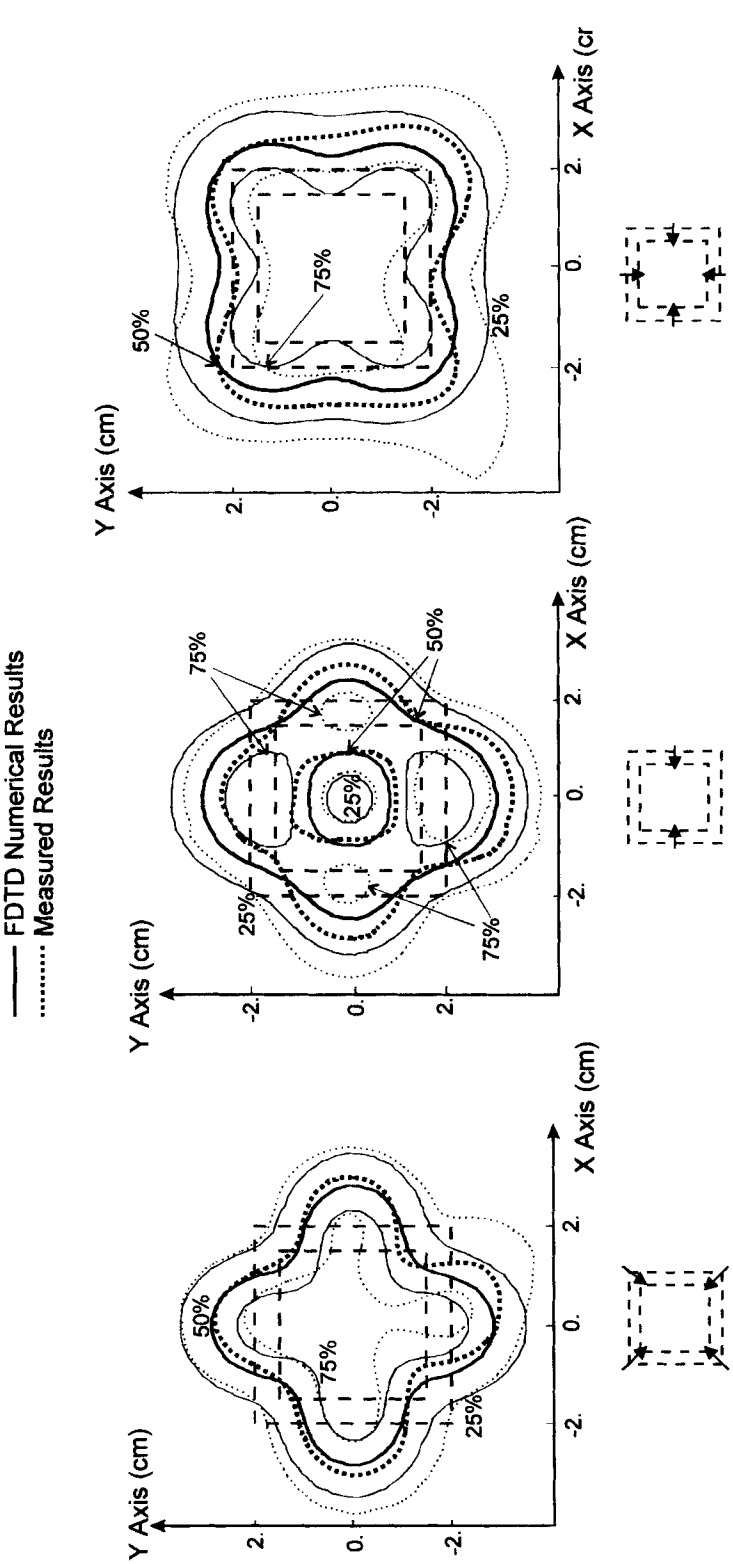

Figure 4. Comparison between theoretical (solid line) and experimental (dotted line) SAR distributions in the 1 cm deep plane for a 4 cm aperture with 5 mm water bolus and dielectrics, for three different feedline excitation configurations: (a) four corner feed; (b) two side feed; and (c) four side feed.

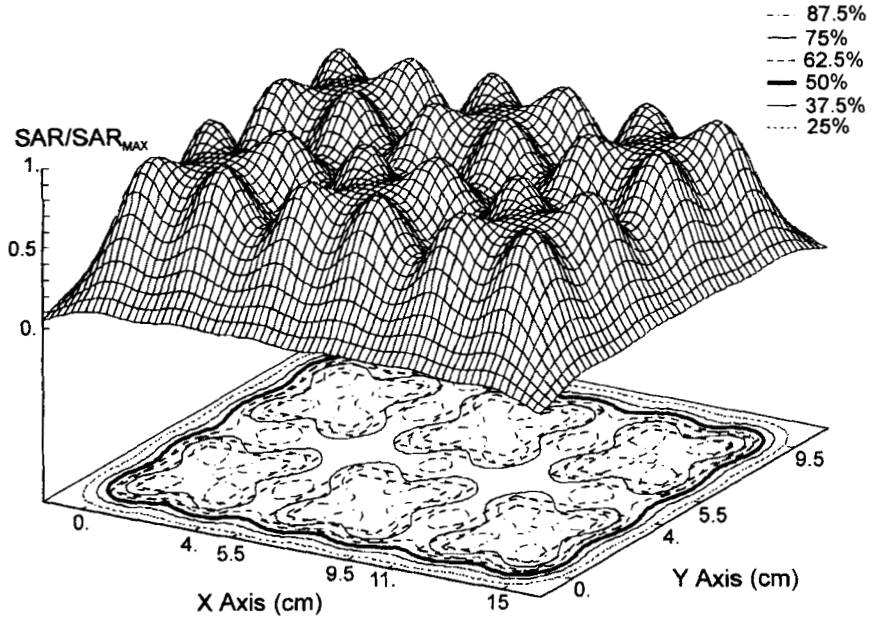

Figure 5. SAR distribution 1 cm deep in muscle for a six element array of 4 cm apertures fed from all four sides and coupled to the load with 5 mm water bolus and interface dielectric layers. Note the close conformance of 50% contour level with the array perimeter.

feedline. Again, the direct comparison in figure 8b shows good agreement between experimental and numerical results for this 2 cm aperture. Figure 9 shows power deposition calculated for the vertical cross section through the centre of the 2 cm aperture. SAR was normalized to the peak value in muscle, obtained at the bolus interface in the same central cross section, just under the excited gap. With the DCC aperture in direct contact with water bolus and muscle load (figure 9a), the 10% SAR contour line reaches down to a depth of 8 mm in muscle. Modelling the complete applicator load with appropriate low ε_r interface dielectics shows increased SAR penetration with the 10% level extending down 1 cm in muscle (figure 9b).

4. Discussion

The FDTD numerical method has been used to characterize radiation patterns from 915 MHz Dual Concentric Conductor applicators intended for hyperthermia treatment of superficial tissue regions extending from the skin surface to a maximum depth of about 1 cm. In previous efforts of this group, the DCC applicator has been modelled in direct contact with either the muscle tissue load or an intervening coupling bolus layer. In practice, the liquid bolus is always contained within a sealed plastic bag ($\varepsilon_r \cong 7$) and a protective coating ($\varepsilon_r \cong 3$) applied to the PCB antenna copper surface. Thus, for the current effort, a more complex FDTD load configuration was implemented to account for the additional thin dielectric interfaces between applicator, bolus, and tissue load. Even with the variable size gridding technique used in these studies, the number of calculation cells for the FDTD model increased by 2.5–3 times and the computer run time by up to 60 times for the same size antenna structure, due to the fine grid necessary to calculate fields in the thin dielectric layers.

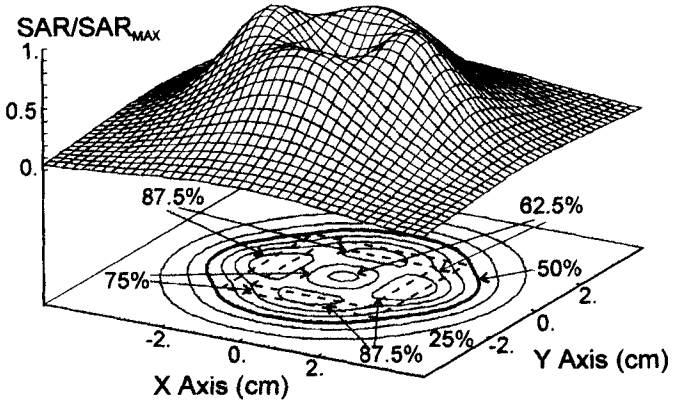

(a)

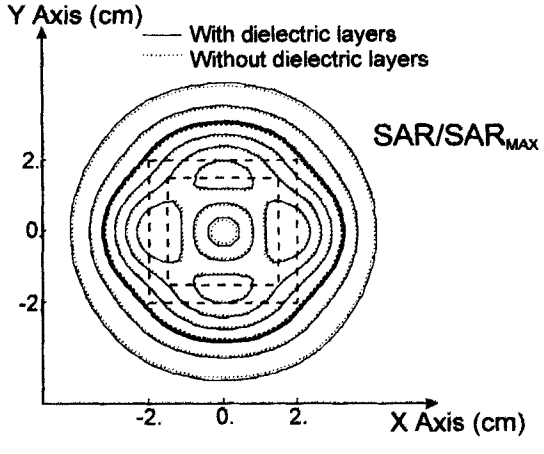

(b)

The necessity of this more complex FDTD model was not immediately obvious. Much of the literature reporting SAR patterns in muscle tissue from microwave antennas has largely ignored the presence of thin dielectric layers. Guy (1971) originally described a widely accepted technique for performance evaluation of microwave antennas using a thermographic camera to assess dT/dt in tissue equivalent phantoms. Kantor and Cetas (1977) described the advantages of using plastic film between sections of the phantom to facilitate thermal imaging of the phantom interior. Since even a thin plastic layer forms an electrically insulating barrier, it was suggested that its use should be limited to cases where the radiating field is parallel to the plastic (Guy *et al.* 1968). This limitation was investigated in detail by Schaubert (1984) who studied the effects of plastic barriers of various thickness on electric fields of various orientation and frequency. He found little effect on either parallel or

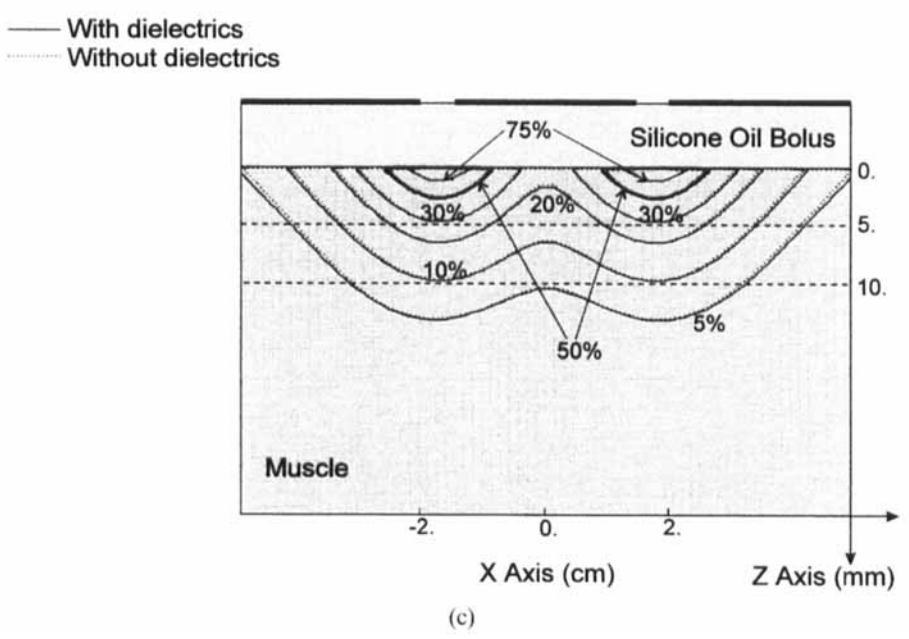

Figure 6. SAR distribution under a 4 cm aperture with two side feed and coupled with 5 mm Silicone Oil bolus. (a) SAR in the 1 cm deep plane calculated with bolus and all interface dielectrics; (b) SAR calculated with (solid) and without (dotted) the interface layers; (c) SAR contours in central vertical cross section with (solid) and without (dotted) dielectric layers. Note there is little difference in SAR for the two load configurations with Silicone Oil bolus. The plot is normalized to 100% SAR_{max} occurring in muscle directly under the source excitation points.

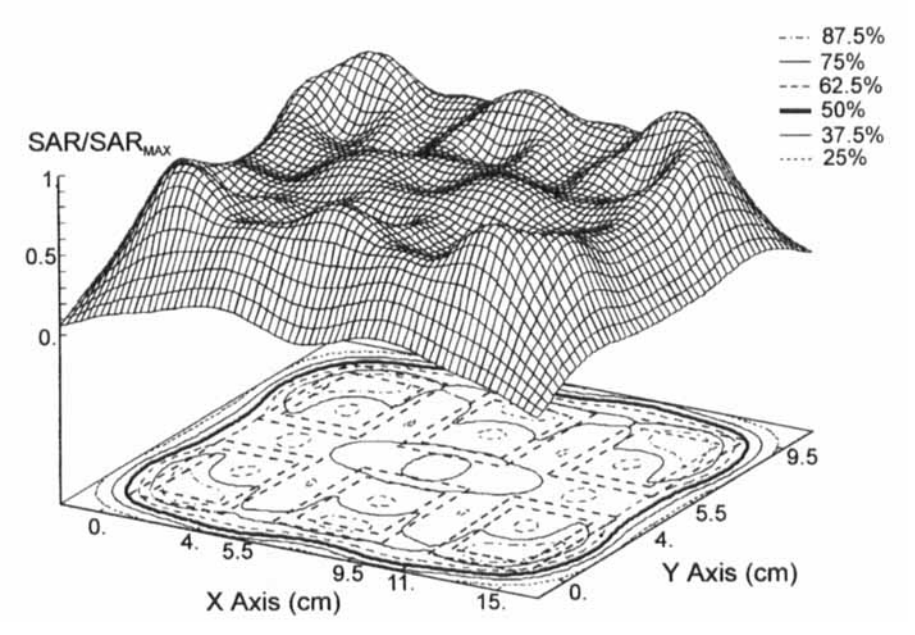

Figure 7. Simulated SAR distribution 1 cm deep in tissue for a six element array of 4 cm apertures excited across two opposing sides and coupled with 5 mm silicon oil bolus.

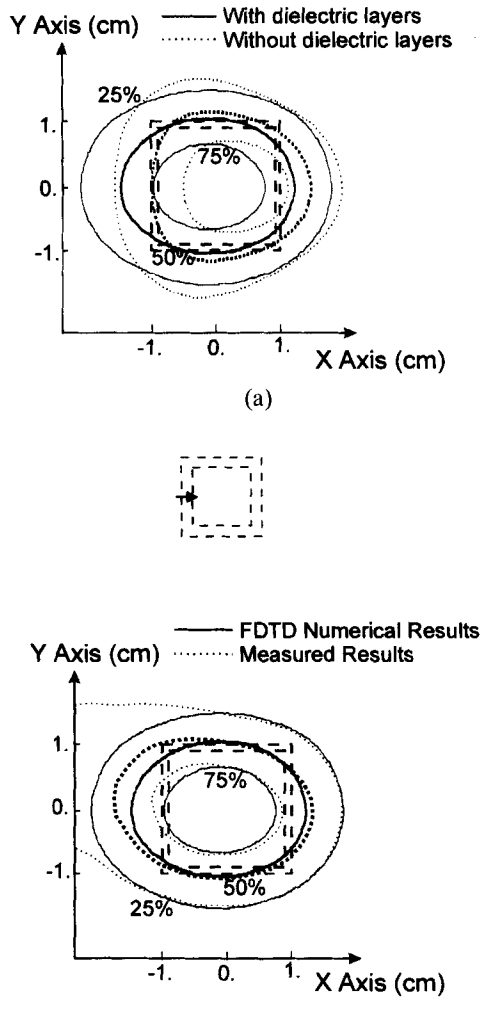

Figure 8. SAR distribution for a 2 cm aperture with 5 mm water bolus and one side (-X direction) feed. (a) FDTD computed SAR contours with (solid) and without (dotted) dielectric layers; (b) SAR obtained numerically (solid) and experimentally (dotted). Note that interface dielectrics improve the symmetry of water coupled applicators.

perpendicularly oriented fields below frequencies of about 800 MHz for insulation thicknesses up to 0.2 mm and an increasing perturbation of the fields (especially the perpendicular orientation) for thicker layers and for frequencies above about 800 MHz. For the conditions of the current study (0.1–0.25 mm dielectric and 915 MHz), these data suggest potentially significant effects on SAR.

During the course of this investigation, it was found that the necessity of using the more computer intensive fine grid model varied dependent on the specific material properties of the coupling bolus and interface layer dielectrics. When DCC apertures are coupled to the tissue load with high $\varepsilon_r = 80$ water bolus, the effect of adding thin $\varepsilon_r = 3$–7 dielectric layers between applicator, bolus, and tissue is significant. The radiation patterns obtained 1 cm deep in muscle show a distinct

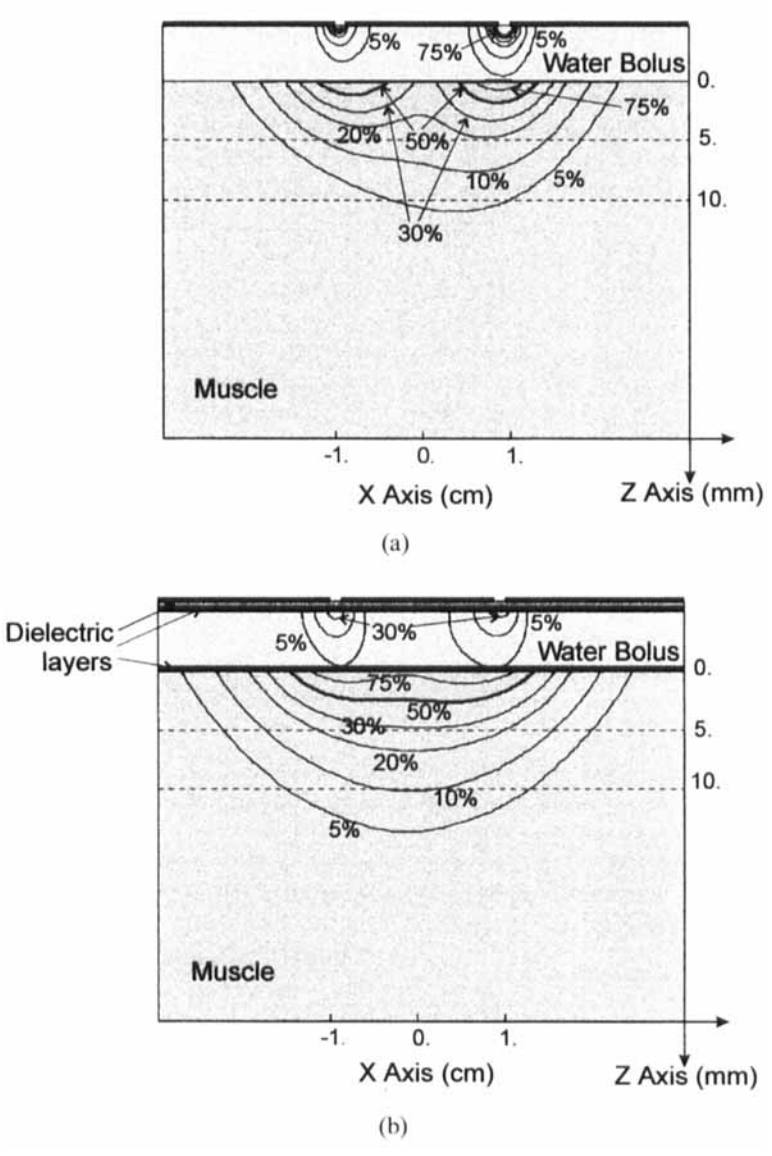

Figure 9. SAR contours under a 2 cm aperture fed across the -x side gap. The vertical x-z plane cross section is taken along the microstrip feedline at the centre of the -x slot. (a) applicator coupled with 5 mm water bolus only; (b) complete load model. Note the increased penetration when interface dielectrics are present. The plots are each normalized to 100% SAR_{max} occurring in the plane shown.

increase in lateral extent, symmetry, and conformance of the 50% SAR_{max} contour to the square aperture outline as compared to the SAR obtained without interface dielectrics, as seen in figures 2 and 8a. In addition, the low ε_r layers increase the penetration of SAR in muscle for water bolus coupled apertures as seen in figures 3 and 9, so that effective penetration becomes similar to that obtained with Silicone Oil coupled apertures (figure 6c). These effects may be readily explained by the big difference in dielectric constants. While the water bolus with $\lambda_{eff} \cong 3.5$ cm at

915 MHz tends to concentrate the fields, the insertion of low ε_r materials with effective wavelenghts of $\lambda_{eff} \cong 12$–18 cm on either side of the water layer layer provides further spreading and smoothing of SAR, suggesting the presence of superficial guided waves in the thin dielectric layers. If silicon oil bolus is used instead of water, these results show that the complete load model is unnecessary since radiation patterns with and without the dielectric layers are essentially identical (figure 6b). This follows because the 5 mm thick Silicone Oil bolus has a dielectric constant ($\varepsilon_r = 2.71$) that is well matched to the interface dielectrics. Thus, the extra low ε_r interface layers included in the complete load model effectively just increase the bolus thickness from 5 to 5.4 mm, producing only a minor additional effect on SAR which is already spread significantly by the 5 mm thick bolus (figure 6). This means that whenever using Silicone Oil bolus, the less complex applicator–bolus–muscle model can be used to calculate SAR from DCC antennas, allowing simulation of larger array structures with less computational requirements than water coupled apertures that require the more complete load model.

Because of the intended application in heating large area superficial disease and the historically large size of previously used waveguide applicators, much of previous work investigated DCC apertures at least 3.5 cm across (Stauffer *et al.* 1994, 1995, 1996). For treatment of smaller tumours, the availability of a compact applicator that can provide more precise control over power deposition is desirable however. For this reason, a smaller 2 cm square DCC applicator was also analysed in this work, completing the more extensive design analysis of that applicator performed without interface dielectrics (Rossetto *et al.* 1997, Stauffer *et al.* 1998). Even more obvious than with larger apertures, correctly modelling the interface layers along with the applicator and water bolus significantly improved the symmetry and lateral extent of SAR as well as the depth of penetration.

With an appropriate FDTD model established and validated with very close correlation to experimentally measured SAR patterns for both 2 and 4 cm aperture sizes, this study returned to it's primary goal of optimizing DCC antenna design with continued FDTD parametric studies. During the examination of electromagnetic excitation possibilities, one, two, and four side feed and four corner feed configurations were characterized. Depending on the aperture size and type of bolus used, different feed configurations were found to provide the best spatial extent, uniformity, symmetry, and conformance of 50% SAR_{max} to the aperture perimeter. For the smallest aperture tested with 2 cm side length representing less than $\lambda_{eff}/2$ in muscle, the simpler to build one side feed configuration pictured in figure 1b was sufficient to provide reasonably symmetric SAR that covered most of the aperture face as long as a 5 mm thick coupling bolus was used (figure 8). For the larger 4 cm aperture, a single side feed produced unacceptable skewing of the field off to the microstrip driven side however. Exciting two opposing sides of the 4 cm aperture as shown in the lower half of figure 1d produced improved symmetry, centring and spreading of the SAR. When coupled to muscle with low ε_r Silicone Oil bolus, the 2 side feed configuration produced very good SAR patterns covering the entire face of single 4 cm apertures (figure 6) as well as the entire perimeter of 1.5 cm spaced six aperture arrays (figure 7). Using a high ε_r bolus, such as more commonly used distilled water, the two side feed configuration was found to leave an unacceptable hole in the centre of the SAR distribution (figure 4b) and between apertures of an array (data not shown). Thus, if water is to be employed for the coupling bolus, it is necessary to use the more complex 4 side microstrip feed network pictured in figure

1d (top) to obtain acceptable heating as demonstrated in figures 2a and 4c, and in six element array configuration (figure 5).

Perhaps most important is that for all aperture sizes and configurations tested, comparison of numerical calculations with experimentally measured SAR distributions demonstrated good agreement, proving the accuracy of the theoretical load model and the FDTD method for detailed analysis of DCC applicators. Availability of this accurate theoretical model provides confidence to complete the design optimization of DCC aperture arrays for hyperthermia treatment of large and small superficial disease.

5. Conclusions

The effect of inserting three additional dielectric layers into the load model used for theoretical calculations of SAR from DCC microwave applicators was investigated using the FDTD numerical method. Radiation patterns were calculated for 2 cm and 4 cm square apertures radiating into muscle through either distilled water or Silicone Oil coupling bolus with associated interface dielectrics, and compared to the SAR distributions obtained from simplified calculations assuming no extra dielectric layers between the applicator, bolus, and tissue. Results demonstrate that for both aperture sizes the complete load model with thin, low ε_r interface dielectrics is advisable when simulating SAR under high ε_r water bolus applicators, but has little benefit for calculating SAR in tissue under a low ε_r Silicone Oil bolus. In order to study the very thin dielectric layers, the spatial discretization must be 2.5–3 times higher and the temporal discretization 5–20 times higher than the simplified load model. This requires significantly longer computation times but allows accurate determination of radiation patterns, as demonstrated by the good agreement between FDTD simulations and experimental SAR measurements for the DCC applicators. These results highlight the usefulness of low ε_r layers between applicator, water bolus, and load to improve the lateral extent, penetration, and centering of SAR under the aperture. Finally, this work clearly demonstrates that 4 cm square DCC apertures can be combined successfully into larger arrays to uniformly heat diffuse, spreading superficial disease.

Acknowledgements

This work was supported by grants from the National Institute of Health RO1 CA-70761 and R43 CA-69868. The authors would also like to acknowledge the careful laboratory assistance of David Wilson and Jon Paul Mahaffey in building and measuring electric field patterns of prototype array applicators. Finally, the authors would like this paper to be dedicated in memory of the late Marco Leoncini whose tireless efforts in the field of electromagnetics contributed to the foundation of this work.

References

CHOU, C. K., MCDOUGALL, J. A., CHAN, K. W., and LUK, K. H., 1990, Evaluation of captive bolus applicators. *Medical Physics*, **17**, 705–709.

DIEDERICH, C. J., and STAUFFER, P. R., 1993, Pre-clinical evaluation of a microwave planar array applicator for superficial hyperthermia. *International Journal of Hyperthermia*, **9**, 227–246.

GOPAL, M. K., HAND, J. W., LUMORI, M. L. D., ALKHAIRI, S., PAULSEN, K. D., and CETAS, T. C., 1992, Current sheet applicator arrays for superficial hyperthermia of chestwall lesions. *International Journal of Hyperthermia*, **8**, 227–240.

GUY, A. W., 1971, Analysis of electomagnetic fields induced in biological tissues by thermographic studies on equivalent phantom models. *IEEE Transactions on Microwave Theory and Techniques*, **19**, 205–214.

GUY, A. W., LEHMANN, J. F., MCDOUGALL, J. A., and SORENSON, C. C., 1968, Studies on therapeutic heating by electromagnetic energy. *Thermal problems in biotechnology*, edited by S. Kezios (New York: American Society of Mechanical Engineers), pp. 26–45.

HARTSGROVE, G., KRASZEWSKI, A., and SUROWIEC, A., 1987, Simulated biological materials for electromagnetic radiation absorption studies. *Bioelectromagnetics*, **8**, 29–36.

KANTOR, G., and CETAS, T. C., 1977, A comparative heating pattern study of direct-contact applicators in microwave diathermy. *Radio Science*, **12**, 111–120.

KAPP, D. S., 1996, Efficacy of adjuvant hyperthermia in the treatment of superficial recurrent breast cancer: confirmation and future directions. *International Journal of Radiation Oncology, Biology and Physics*, **35**, 1117–1121.

LEE, E. R., 1995, Electromagnetic Superficial Heating Technology. *Thermoradiotherapy and Thermochemotherapy, Vol. 1: Biology, Physiology, and Physics*, edited by M. H. Seegenschmiedt, P. Fessenden and C. C. Vernon (Berlin, Heidelberg: Springer-Verlag), pp. 193–217.

MANFRINI, V., STAUFFER, P. R., LEONCINI, M., and DIEDERICH, C. J., 1995, Dual concentric conductor arrays for microwave hyperthermia: theoretical study of design parameters. *Proceedings of Wescon/95*, San Francisco (Piscataway, NJ: IEEE Press), pp. 662–667.

OVERGAARD, J., GONZALES GONZALES, D., HULSHOF, M. C. C. H., ARCANGELI, G., DAHL, O., MELLA, O., and BENTZEN, S. M., 1996, Hyperthermia as an adjuvant to radiation therapy of recurrent or metastatic malignant melanoma. A multicentre randomized trial by the European Society for Hyperthermia Oncology. *International Journal of Hyperthermia*, **12**, 3–20.

ROSSETTO, F., STAUFFER, P. R., DIEDERICH, C. J., DEARDORFF, D., BIFFI GENTILI, G., and LEONCINI, M., 1997, FDTD characterization of radiation patterns from flexible microstrip applicators. *Proceedings of IEEE Antennas and Propagation Society Symposium Digest*, Montreal, Canada, Volume 3 (IEEE Press, Piscataway, NJ), pp. 1562–1565.

SCHAUBERT, D. H., 1984, Electromagnetic heating of tissue-equivalent phantoms with thin, insulating partitions. *Bioelectromagnetics*, **5**, 221–232.

SNEED, P. K., and PHILLIPS, T. L., 1991, Combining hyperthermia and radiation: how beneficial? *Oncology*, **5**, 99–108.

STAUFFER, P. R., DIEDERICH, C. J., and BOZZO, D., 1994, Conformal array microwave applicator for superficial hyperthermia of large contoured surfaces. *1994 IEEE MTT-S International Microwave Symposium Digest*, **1**, 531–534.

STAUFFER, P. R., LEONCINI, M., MANFRINI, V., GENTILI, G. B., DIEDERICH, C. J., and BOZZO, D., 1995, Dual concentric conductor radiator for microwave hyperthermia with improved field uniformity to periphery of aperture. *IEICE Transactions on Communications*, **E78-B**, 826–835.

STAUFFER, P. R., MANFRINI, V., LEONCINI, M., and DIEDERICH, C. J., 1996, Microwave array applicator for superficial hyperthermia of large contoured surfaces. *Proceedings of International Congress of Hyperthermic Oncology*, Roma, Italy, Volume II, edited by C. Franconi, G. Arcangeli and R. Cavaliere, pp. 467–469.

STAUFFER, P. R., ROSSETTO, F., LEONCINI, M., and BIFFI GENTILLI, G., 1998, Radiation patterns of dual concentric conductor microstrip antennas for superficial hyperthermia. *IEEE Transactions on Biomedical Engineering*, **45** 605–613.

STRAUBE, W. L., MYERSON, R. J., EMAMI, B., and LEYBOVICH, L. B., 1990, SAR patterns of external 915 MHz microwave applicators. *International Journal of Hyperthermia*, **6**, 665–670.

STUCHLY, M. A., KRASZEWSKI, A., and STUCHLY, S. S., 1984, Implantable electric-field probes—some performance characteristics. *IEEE Transactions on Biomedical Engineering*, **31**, 526–531.

TAFLOVE, A., 1980, Application of the finite-difference time-domain method to sinusoidal steady-state electromagnetic penetration problems. *IEEE Transactions on Electromagnetic Compatibility*, **22**, 191–202.

UMASHANKAR, K., and TAFLOVE, A., 1982, A novel method to analyze electromagnetic scattering of complex objects. IEEE Transactions on Electromagnetic Compatibility, **4**, 397–405.

VERNON, C. C., HAND, J. W., FIELD, S. B., MACHIN, D. WHALEY, J. B., VAN DER ZEE, J., VAN PUTTEN, W. L. J., VAN RHOON, G. C., VAN DIJK, J. D. P., GONZALEZ-GONZALEZ, D., LIU, F. F., GOODMAN, P., and SHERAR, M., 1996, Radiotherapy with or without hyperthermia in the treatment of superficial localized breast cancer: Results from five randomized controlled trials. *International Journal of Radiation Oncology, Biology and Physics*, **35**, 731–744.

YEE, K. S., 1966, Numerical solution of initial boundary value problems involving Maxwell's equations in isotropic media. *IEEE Transactions on Antennas and Propagation*, **AP-14**, 302–307.